Dynamic near-field calculations of surface-plasmon polariton pulses resonantly scattered at sub-micron metal defects

José A. Sánchez-Gil
Instituto de Estructura de la Materia, Consejo Superior de Investigaciones Científicas, Serrano 121, E-28006 Madrid, Spain
j.sanchez@iem.cfmac.csic.es

Alexei A. Maradudin
Department of Physics and Astronomy and Institute for Surface and Interface Science, University of California, Irvine, CA 92697
aamaradu@uci.edu

Abstract: We investigate theoretically the near-field dynamics of the scattering of a surface-plasmon polariton (SPP) pulse impinging normally on a rectangular groove on an otherwise planar metal surface. Our formulation is based on solving the reduced Rayleigh equation (derived through the use of an impedance boundary condition) for every component of the spectral decomposition of the incoming SPP pulse. Numerical calculations are carried out of the time dependence of the near-field resonant scattering effects produced at the rectangular groove. The scattering process is tracked through the (time-resolved) repartition of the incoming SPP electromagnetic energy into reflected and transmitted SPP pulses, and into pulsed scattered light. Furthermore, we directly show evidence of the excitation of single resonances, as manifested by the concentration of electric field intensity within the groove, and its subsequent leakage, over the resonance lifetime. The near-field formation of oscillations caused by the interference between two adjacent resonances simultaneously excited is also considered.

© 2004 Optical Society of America

OCIS codes: (240.6680) Surface plasmons; (260.5740) Resonance; (290.5880) Scattering, rough surfaces; (320.2250) Femtosecond phenomena

References and links

1. T. A. Leskova and N. I. Gapotchenko, "Fabry-Perot type interferometer for surface polaritons: resonance effects," Solid State Commun. **53**, 351 (1985).
2. B. Rothenhäusler and W. Knoll, "Surface plasmon interferometry in the visible," Appl. Phys. Lett. **52**, 1554 (1988).
3. B. Rothenhäusler and W. Knoll, "Interferometric determination of the complex wave vector of plasmon surface polaritons," J. Opt. Soc. Am. B **5**, 1401 (1988).
4. F. Pincemin, A. A. Maradudin, A. D. Boardman, and J.-J. Greffet, "Scattering of a surface plasmon polariton by a surface defect," Phys. Rev. B **50**, 15261 (1994).
5. A. V. Shchegrov, I. V. Novikov, and A. A. Maradudin, "Scattering of surface plasmon polaritons by a circularly symmetric surface defect," Phys. Rev. Lett. **78**, 4269 (1997).
6. J. A. Sánchez-Gil, "Surface defect scattering of surface plasmon polaritons: Mirrors and light emitters," Appl. Phys. Lett. **73**, 3509 (1998).

#3513 - $15.00 US Received 12 December 2003; revised 27 February 2004; accepted 27 February 2004

7. J. A. Sánchez-Gil and A. A. Maradudin, "Near-field and far-field scattering of surface plasmon polaritons by one-dimensional surface defects," Phys. Rev. B**60**, 8359 (1999).
8. T. A. Leskova, A. A. Maradudin, and W. Zierau, "Surface plasmon polariton propagation near an index step," Proc. SPIE **4100**, 1 (2000).
9. Z. Schlesinger and A. J. Sievers, "Infrared surface wave interferometry," Appl. Phys. Lett. **36**, 409 (1980).
10. B. Rothenhäusler and W. Knoll, "On the influence of the propagation length of plasmon surface polaritons in the visible energy range for the optical characterization of heterogeneous thin films," Surf. Sci. **191**, 585 (1987).
11. B. Rothenhäusler and W. Knoll, "Total internal diffraction of plasmon surface polaritons," Appl. Phys. Lett. **51**, 783 (1987).
12. B. Rothenhäusler and W. Knoll, "Surface plasmon microscopy," Nature **332**, 615 (1988)
13. C. E. H. Berger, R. P. H. Koioyman, and J. Greve, "Surface plasmon propagation near an index step," Opt. Commun. **167**, 183 (1999).
14. I. Smolyaninov, D. L. Mazzoni, and C. C. Davis, "Imaging of surface plasmon scattering by lithographically created individual surface defects," Phys. Rev. Lett. **78**, 2823 (1997).
15. I. I. Smolyaninov, D. L. Mazzoni, J. Mait, and C. C. Davis, "Experimental study of surface plasmon scattering by individual surface defects," Phys. Rev. B **56**, 1601 (1997).
16. A. Dogariu, T. Thio, L. J. Wang, T. W. Ebbesen, and H. J. Lezec, "Delay in light transmission through small apertures," Opt. Lett. **26**, 450 (2001).
17. Y.-H. Liau, S. Egusa, and N. F. Scherer, "Ultrafast interferometric measurements of plasmonic transport in photonic crystals," Opt. Lett. **27**, 857 (2002).
18. J. A. Sánchez-Gil and A. A. Maradudin, "Resonant scattering of surface-plasmon polariton pulses by nanoscale metal defects," Opt. Lett. **28**, 2255 (2003).
19. H. Raether, *Surface Polaritons on Smooth and Rough Surfaces and on Gratings* (Springer-Verlag, Berlin, 1988).
20. A. A. Maradudin, "An impedance boundary condition for a rough surface," in *Topics in Condensed Matter Physics*, ed. M. P. Das (Nova, New York, 1994), p. 33.
21. Note that, strictly speaking, such a linear mapping of the surface corrugation into the surface impedance on the plane may not be correct, as discussed in Ref. [7], in the case of rectangular defects, due to the influence of higher-order terms in the slope. Nonetheless, this should not affect the results for the resonant scattering process, except for, presumably, the actual position and strength of resonances.
22. In our two-dimensional geometry, a near-field area at constant height converts into a single line; we actually merge in a single map all such line scans, from the vacuum-metal interface up to a certain, maximum height.
23. We have verified that both resonances are decoupled by separately probing each with surface plasmon polariton pulses appropriately tuned.
24. W. L. Barnes, A. Dereux, and T. W. Ebbesen, "Surface plasmon sub-wavelength optics," Nature **424**, 824 (2003).

1. Introduction

There have been several theoretical studies of the scattering of surface plasmon polaritons by isolated defects of various types on an otherwise planar metal surface [1, 2, 3, 4, 5, 6, 7, 8], as well as several experimental studies of such scattering processes [2, 3, 9, 10, 11, 12, 13, 14, 15]. In all of this work continuous wave excitation of the incident surface plasmon polariton (SPP) was assumed, i.e. the incident SPP was assumed to be monochromatic. This precluded the observation of any dynamic effects associated with these scattering processes, such as delay times associated with the resonant scattering of a SPP pulse from a localized surface defect. Recent experimental time-domain studies on the transmission of pulsed light through small apertures [16], and on SPP transport in a two-dimensional surface plasmon polaritonic crystal [17] have been reported, demonstrating the feasibility of such measurements in contexts where SPPs play a dominant role. On the theoretical side, the dynamics of the resonant scattering of SPP pulses by isolated nanoscale defects were investigated through calculations of the time dependence of the reflected and transmitted SPPs, and of the angular distribution of the intensity of the scattered light [18]. The resonant nature of the scattering was manifested through the exponential tails of the scattered SPPs, and by the delay time of the transmitted SPP pulse.

In this paper we investigate theoretically the near-field dynamics of the scattering of a SPP pulse incident normally on a rectangular groove on an otherwise planar metal surface. The choice of a rectangular groove instead of the Gaussian groove studied in [18] is due to the fact that a rectangular groove possesses electromagnetic resonances that are spectrally denser and

#3513 - $15.00 US Received 12 December 2003; revised 27 February 2004; accepted 27 February 2004
(C) 2004 OSA

narrower, i.e. have longer lifetimes, than the resonances supported by a Gaussian groove of a similar size or even deeper. However, for purposes of comparison we also present results for the near electric field intensity close to the defect, calculated for the Gaussian groove studied in [18]. We calculate the time dependence of the SPP pulses reflected from and transmitted through the rectangular groove, together with the time dependence of the field scattered into the vacuum above the metal surface. We are particularly interested in these time dependences when the central frequency of the incident SPP pulse is close to the frequency of one of the resonances supported by the groove, or close to the frequencies of a pair of spectrally close resonances. We also calculate the electric near-field intensity close to the rectangular groove under resonance conditions. These results are obtained from a numerical solution of the reduced Rayleigh equation for the single nonzero component of the magnetic vector in the vacuum region, derived through the use of an impedance boundary condition, for each component in the spectral decomposition of the incident SPP pulse. They enable the frequencies of the resonances studied to be determined, together with their lifetimes, among other features of the time dependence of the scattering of SPP pulses from a surface profile line defect. Although our analysis is restricted to one-dimensional defects, we emphasize that many of the resulting dynamical effects can be qualitatively extrapolated to two-dimensional defects.

The outline of this paper is as follows. In Section 2 we formulate the problem of the scattering of a SPP pulse by a surface defect and describe how it is solved. In Section 3 this formulation is applied to the scattering of the pulse from a rectangular groove when the central frequency of the pulse is close to the frequency of one of the resonances supported by the groove. The scattering from the same rectangular groove of a pulse with a lower frequency and larger spectral width that simultaneously excites two spectrally close resonances supported by the groove is also investigated in this section. For the sake of comparison, in Section 4 the time dependence of the near-field intensity for the resonant scattering of SPP pulse by a Gaussian groove with parameters corresponding to the resonance studied in [18] is calculated. The conclusions drawn from our calculations are presented in Section 5.

2. Pulsed SPP scattering model

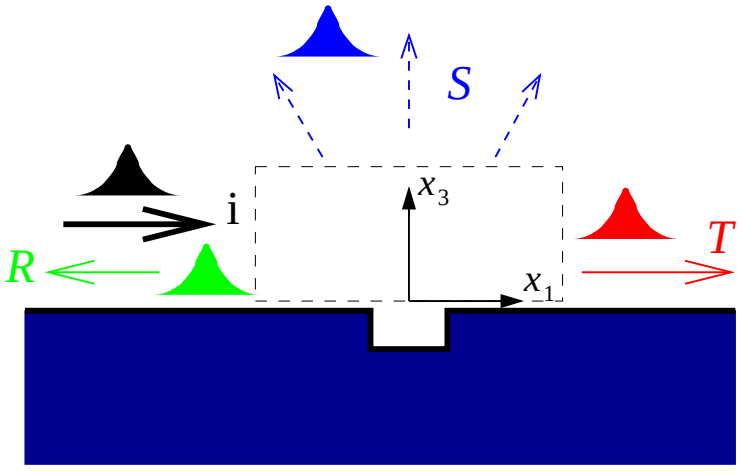

Fig. 1. Illustration of the scattering geometry. The dashed rectangle shows the configuration of the near-field region scanned in Figs. 3, 4, 7 and 9.

The scattering geometry is depicted in Fig. 1. A pulsed SPP propagating on a planar vacuum-

#3513 - $15.00 US Received 12 December 2003; revised 27 February 2004; accepted 27 February 2004
(C) 2004 OSA

silver interface ($x_3 = 0$, the semi-infinite metal occupying the lower half-space) in the positive x_1 direction impinges from the negative x_1 axis on a line defect characterized by its profile function $x_3 = f(x_1)$ (constant along the x_2 axis) and located at the origin. The incident p-polarized SPP pulse is characterized by its only non-zero component of the magnetic field in vacuum,

$$H_2^{(i)}(x_1,x_3;t) = \int_{-\infty}^{\infty} \mathrm{d}\omega F(\omega) \exp[ik(\omega)x_1 - \beta_0(\omega)x_3] \exp(-i\omega t), \quad (1)$$

$$F(\omega) = \exp[-(\omega^2-\omega_0^2)/(\Delta\omega)^2]/(\sqrt{\pi}\Delta\omega), \quad (2)$$

with a Gaussian spectral amplitude $F(\omega)$. $k(\omega)$ and $\beta_0(\omega)$ are the SPP wave vector components [19]; since we make use of the impedance boundary condition on a plane [20] in the theoretical formulation of this problem, these components are given by:

$$k(\omega) = \frac{\omega}{c}\left(1 - \frac{1}{\varepsilon(\omega)}\right)^{1/2}, \beta_0(\omega) \equiv \left(k(\omega)^2 - \frac{\omega^2}{c^2}\right)^{1/2} = \frac{\omega}{c}[-\varepsilon(\omega)]^{-1/2}, \quad (3)$$

where $\varepsilon(\omega)$ is the metal dielectric function.

The time-dependent scattered field in the vacuum half-space can be written in the form of a Rayleigh (plane wave) expansion:

$$H_2^{(sc)}(x_1,x_3;t) = \int_{-\infty}^{\infty} \mathrm{d}\omega F(\omega) e^{-i\omega t} \int_{-\infty}^{\infty} \frac{\mathrm{d}q}{2\pi} R(q,\omega) \exp[i(qx_1 + \alpha_0(q,\omega)x_3)], \quad (4)$$

with $\alpha_0(q,\omega) \equiv (\omega^2/c^2 - q^2)^{1/2}$, and $R(q,\omega)$ the scattering amplitude for a monochromatic wave of frequency ω. It is shown in Ref. [7], upon imposing the impedance boundary condition on a plane, that the scattering amplitude can be written in the form

$$R(q,\omega) = G_0(q,\omega)T(q,\omega), \quad (5)$$

where $G_0(q,\omega)$ is the Green's function of the SPP on the unperturbed surface

$$G_0(q,\omega) = \frac{i\varepsilon(\omega)}{\varepsilon(\omega)\alpha_0(q,\omega) + i(\omega/c)[-\varepsilon(\omega)]^{1/2}} \equiv C(q,\omega)\left(\frac{1}{q-k(\omega)} - \frac{1}{q+k(\omega)}\right), \quad (6)$$

where the matrix $T(q,\omega)$ satisfies the equation

$$T(q,\omega) = V(q|k(\omega)) + \int_{-\infty}^{\infty} \frac{dp}{2\pi} V(q|p) G_0(p,\omega) T(p,\omega), \quad (7)$$

and the scattering potential $V(q|p)$ is connected to the surface impedance $s(x_1)$ through

$$V(q|p) \equiv \beta_0(\omega)\hat{s}(q-p), \qquad \hat{s}(Q) = \int_{-\infty}^{\infty} dx_1\, e^{-iQx_1} s(x_1). \quad (8)$$

At a sufficiently large distance from the defect on the interface, the resulting (incident plus scattered) magnetic field, Eqs. (2) and (4), can be written in the form of reflected and transmitted SPP pulses:

$$H_2(x_1,0;t) = H_2^{(i)}(x_1,0;t) + H_2^{(r)}(x_1,0;t)$$
$$= H_2^{(i)}(x_1,0;t) + \int_{-\infty}^{\infty} \mathrm{d}\omega F(\omega) e^{-i\omega t} \rho(\omega) \exp[-ik(\omega)x_1 - \beta_0(\omega)x_3], \; x_1 \ll 0; \quad (9)$$

$$H_2(x_1,0;t) = H_2^{(t)}(x_1,0;t)$$
$$= \int_{-\infty}^{\infty} \mathrm{d}\omega F(\omega) e^{-i\omega t} \tau(\omega) \exp[ik(\omega)x_1 - \beta_0(\omega)x_3], \; x_1 \gg 0, \quad (10)$$

#3513 - $15.00 US Received 12 December 2003; revised 27 February 2004; accepted 27 February 2004
(C) 2004 OSA

where $\rho(\omega)$ and $\tau(\omega)$ are, respectively, the monochromatic SPP reflection and transmission amplitudes [7]:

$$\rho(\omega) = iT(-k^R(\omega),\omega)\,C(-k^R(\omega),\omega) \quad (11)$$

$$\tau(\omega) = 1+iT(k^R(\omega),\omega)\,C(k^R(\omega),\omega), \quad (12)$$

with $k^R(\omega)$ denoting the real part of $k(\omega)$.

The time-dependent field scattered into the far field in the vacuum region can be calculated from Eq. (4) with $(x_1,x_3)\equiv(r\cos\theta,r\sin\theta)$ (where θ is the scattering angle) in the limit that $r\gg\lambda$ by means of the method of stationary phase. The resulting expression has the form of propagating pulses of outgoing cylindrical waves:

$$H_2^{(s)}(r,\theta;t)=\frac{e^{-i\frac{\pi}{4}}\cos\theta}{\sqrt{2\pi r}}\int_{-\infty}^{\infty}\mathrm{d}\omega F(\omega)e^{-i\omega t}\sqrt{\frac{\omega}{c}}R((\omega/c)\sin\theta,\omega)\exp\left(i\omega\frac{r}{c}\right), \quad (13)$$

from which the following time-dependent angular distribution of the scattered intensity is defined:

$$I(\theta,t)\equiv r\,|H_s|^2\,. \quad (14)$$

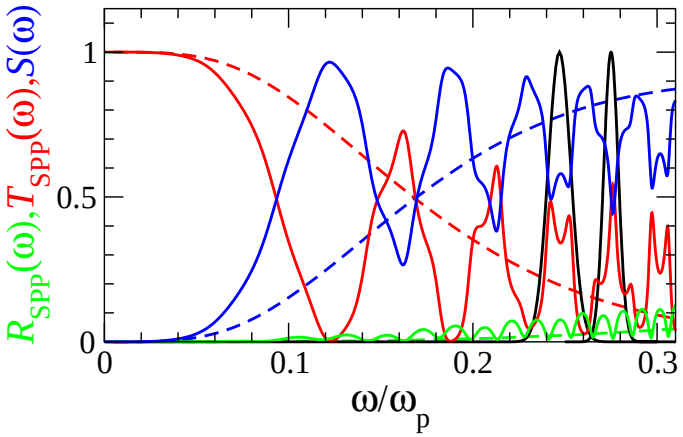

Fig. 2. Spectral dependence of the monochromatic, SPP reflection (green curve) and transmission (red curve) coefficients (R_{SPP} and T_{SPP}, respectively), and total radiated energy S (blue curve) for a rectangular defect of half-width $L=789$ nm. Solid curves: Groove, $h=-157$ nm; Dashed curves: Ridge, $h=157$ nm. $\lambda_p=2\pi c/\omega_p=157$ nm (Ag). The spectral amplitudes (normalized to 1) of the SPP pulses considered below are superimposed (black curves).

The numerical calculations are based on solving the reduced Rayleigh equation (7), as detailed in Ref. [7], for each spectral component of the incident SPP pulse. Then the corresponding Fourier transforms yield the reflected and transmitted SPP pulses, Eqs. (9) and (10), and also the time dependence of the scattered far field, Eqs. (13) and (14). The calculations of the time evolution of the near field intensity are carried out on the basis of the electric field derived (through the $\nabla\times\mathbf{H}$ Maxwell equation) from the (incident plus scattered) magnetic field, Eqs. (2) and (4). In what follows, the metal substrate is assumed to be silver, its dielectric function given by Drude's formula $\varepsilon(\omega)=1-\omega_p^2/\omega^2$, with $\lambda_p\equiv 2\pi c/\omega_p=157$ nm. It is well known that for frequencies in the visible and near IR below the onset of the strong ohmic losses

#3513 - $15.00 US Received 12 December 2003; revised 27 February 2004; accepted 27 February 2004
(C) 2004 OSA

associated with interband transitions (at $\lambda \sim 400$ nm for Ag), Drude's free-electron approximation correctly describes the metal response. In addition, we neglect the absorptive contribution to Drude's formula, since the corresponding SPP inelastic mean free path ℓ_{abs} is much larger than the defect size (e.g. $\ell_{abs} \sim 24\,\mu$m for Ag at $\lambda = 650$ nm); thus no significant effects are expected in the scattering process [5] other than dissipative losses in the SPP propagation.

3. Rectangular groove

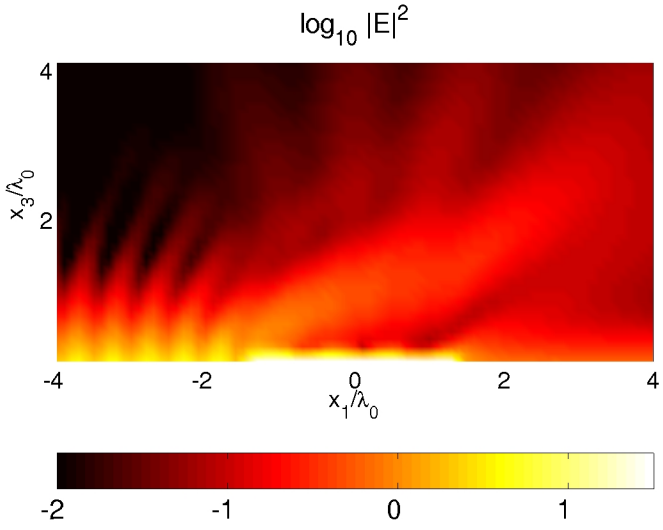

Fig. 3. (308 KB) Movie of the time evolution of the near (electric) field intensity (log scale) images in an area of $8\lambda \times 4\lambda$ perpendicular to the Ag surface for a rectangular groove (located at the bottom center, see Fig. 1) of half-width $L = 785$ nm and depth $h = -157$ nm. The incident SPP pulse parameters are: $\omega_0/\omega_p = 0.275$ ($\lambda_0 = 571$ nm) and $\Delta\omega/\omega_0 = 0.02$. Front picture: $t = 0$ (incoming SPP pulse maximum at $x_1 = 0$).

It has been shown that Gaussian grooves, unlike ridges, exhibit resonances that can be probed in the far field through pulsed SPP scattering [18]. However, for the near field calculations shown below, we use the surface defect impedance in the form of a rectangular groove of half-width L and depth $|h|$,

$$s(x_1,\omega) \quad = \quad \frac{1-\varepsilon(\omega)}{d(\omega)\varepsilon(\omega)} h[\Theta(x_1+L)-\Theta(x_1-L)], \tag{15}$$

where $h<0$, $d(\omega) = c[\varepsilon(\omega)]^{-1/2}/\omega$ is the skin depth, and $\Theta(u)$ is the Heaviside unit step function. The frequency dependent factor in Eq. (15) is introduced, following Ref. [20], in order to preserve the connection between surface impedance and actual corrugation to lowest order in both the defect height and slope [21]. Rectangular grooves possess several resonances, spectrally denser and narrower than those supported by Gaussian grooves of a similar size, or even deeper.

This is evident from the spectral dependence of the SPP reflection and transmission coefficients ($R_{\rm SPP} \equiv |\,\rho\,|^2, T_{\rm SPP} \equiv |\,\tau\,|^2$), and of S, the total, normalized power carried away from the surface in the form of volume electromagnetic waves (obtained by integrating over θ

#3513 - $15.00 US Received 12 December 2003; revised 27 February 2004; accepted 27 February 2004
(C) 2004 OSA

the differential reflection coefficient [7]), presented in Fig. 2 for $h = -\lambda_p = -157.1$ nm and $L = 5\lambda_p = 785$ nm. (Incidentally, the results corresponding to a rectangular ridge with identical parameters ($h > 0$), also shown here, reveal no evidence of resonances, with structureless, monotonic spectral variations qualitatively similar to those of Gaussian ridges [18].) Resonant frequencies are obtained from the behavior of both the SPP transmission amplitude $\tau(\omega)$ and the complex zeroes of the corresponding homogeneous reduced Rayleigh equation [Eq. (7) without the independent term], exhibiting a complicated pattern that cannot be readily fitted to a sum of well defined Lorentzians $\tau(\omega) \propto \Gamma/[\omega - (\omega_R - i\Gamma)]$, but is still roughly attributable to the transmission peaks in Fig. 2.

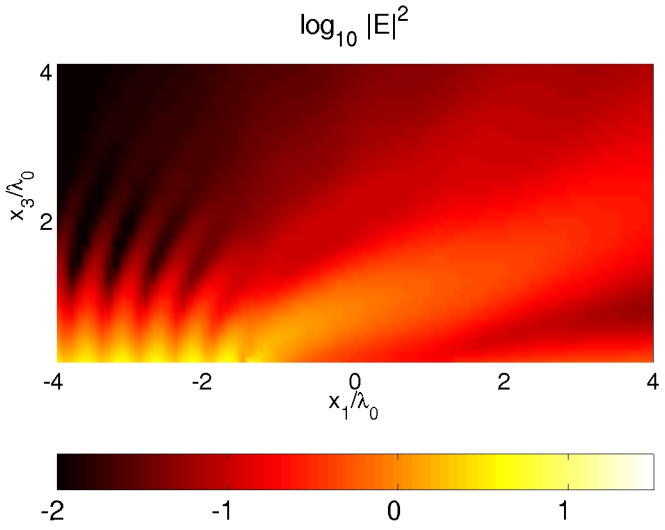

Fig. 4. (260 KB) Same as in Fig. 3 but for a rectangular ridge ($h = 157$ nm).

3.1. Single resonance

We now calculate the time dependence of the electric near-field intensity close to the defect at resonant conditions. Thus we consider an incident SPP pulse with $\omega_0/\omega_p = 0.275$ (λ_0 =571 nm) and spectral width $\Delta\omega/\omega_0 = 0.02$ (FWHM$\sim$ 60 fs) as shown in Fig. 2, where it is clearly seen that the pulse spectral envelope covers (only) the resonance at $\omega_0/\omega_p = 0.275$. Dynamic near-field maps [22] are presented in the movie of Fig. 3 in a logarithmic scale. At negative times, only the evanescent field of the approaching SPP pulse located to the left of the defect is observed. At $t = 0$ (the peak of the incoming SPP pulse right at the center of the defect), the signatures of the scattering process appear in several ways: a reflected SPP that interferes with the incoming pulse and yields the observed fringes to the left of the defect; propagating waves that are scattered into the vacuum with a characteristic angular pattern (discussed below); and the evanescent field of the transmitted SPP seen to the right of the defect. These signatures differ from one defect (or SPP central frequency) to another, revealing the peculiarities of the scattering process for each case. At a certain positive time, the central parts of the reflected and transmitted SPP, and also of the scattered light, are displaced towards their corresponding propagation directions. Finally, all of them should be out of the range of the maps at $t > x_{max}/v_{SPP}$ [where the SPP group velocity is given from Eq. (3) by $v_{\rm SPP}/c = (\omega/(ck(\omega)))^3$]. However, as

#3513 - $15.00 US Received 12 December 2003; revised 27 February 2004; accepted 27 February 2004
(C) 2004 OSA

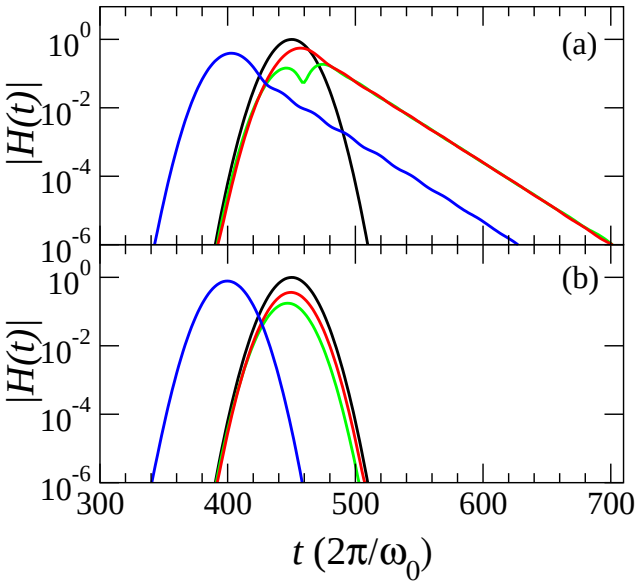

Fig. 5. Pulse amplitudes for $\omega_0/\omega_p = 0.275$ and $\Delta\omega/\omega_0 = 0.035$ at a distance $x = 400\lambda_0$ scattered from rectangular defects of half-width $L = 785$ nm and height $h = \pm 157$ nm: Reflected (green curve) and transmitted (red curve) SPP, and radiated (blue curve) at $\theta = \theta_{max}$. (a) Groove, $\theta_{max} = 46.6^\circ$; (b) Ridge, $\theta_{max} = 62.5^\circ$. The freely propagating SPP pulse is also shown (black curve).

a consequence of the excitation of the resonance in the rectangular groove (see Fig. 2), EM energy is stored in the defect that leaks out, even long after the SPP incoming pulse is gone, in the form of reflected and transmitted SPP (the reflected SPP is weak), and scattered light, with typical decay times given by the resonance lifetime; as discussed below, the latter must be longer than the SPP pulse width for this resonant leakage to be observable.

For the sake of comparison, we show in the movie of Fig. 4 the dynamic near-field maps for a rectangular ridge with identical parameters (except that $h > 0$). Although the scattering process at times $t \leq (\Delta\omega)^{-1}$ is qualitatively similar to that in Fig. 3 (of course, with a different energy balance for the outgoing channels), no resonance is excited at the defect, however. Thus no particular features are observed in the near electric field intensity at times after the central lobes of the reflected and transmitted SPP and of the scattered light leave the scene.

The corresponding reflected and transmitted SPP pulses at a distance $d = 400\ (2\pi c/\omega_0)$ from the defect are shown in Fig. 5 for both the rectangular groove and ridge; Also included is the time-dependence of the scattered light amplitude $r^{1/2}\,|H_s|$ at the same distance and given scattering angle $\theta = \theta_{max}$ (at which the corresponding angular distribution of scattered power is maximum). In the case of the rectangular groove at resonance, Fig. 5(a), the negative exponential tails of all the pulses quantitatively confirm the resonant scattering process described in the movie of Fig. 3. By fitting the tails to $\exp(-t\Gamma)$, with linewidth $\Gamma/\omega_0 = 8.7 \cdot 10^{-3} \pm 10^{-5}$, the resonance lifetime is obtained (time decay $\Gamma^{-1} \approx 35$ fs). This value is in fairly good agreement with the resonance HWHM as inferred from $T_{\rm SPP}(\omega)$. The resonance life time can be also probed through the delay time of the transmitted SPP with respect to the freely propagating SPP, more accurately determined by calculating the cross-correlation with longer pulses [18].

In addition to the resonant tails, there are other interesting features in Fig. 5(a) exhibiting the complex, highly dispersive response of the rectangular groove. The transmitted SPP pulse is

#3513 - $15.00 US Received 12 December 2003; revised 27 February 2004; accepted 27 February 2004
(C) 2004 OSA

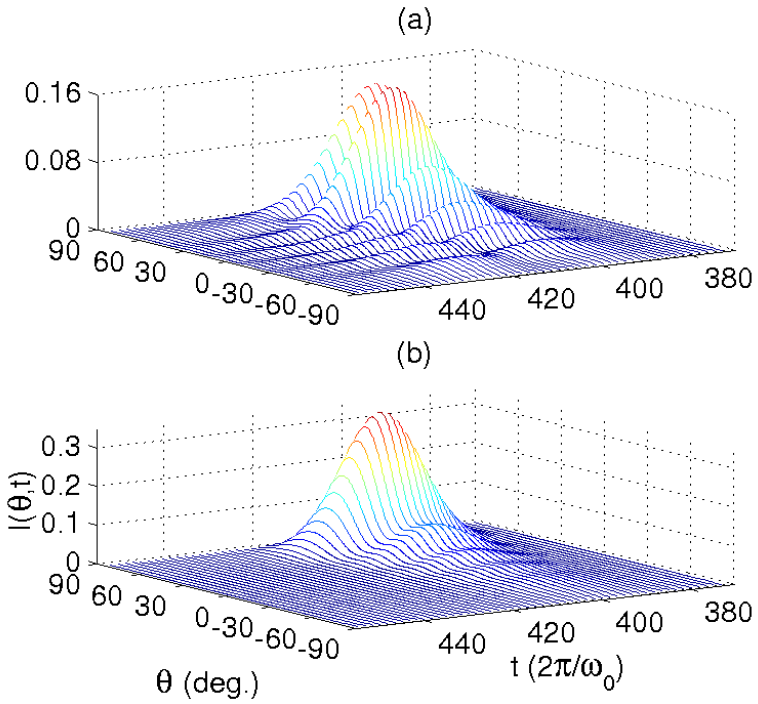

Fig. 6. Time dependence of the angular distribution of intensity scattered (for $\omega_0/\omega_p = 0.275$) from rectangular defects of half-width $L = 785$ nm and height $h = \pm 157$ nm. (a) Groove; (b) Ridge.

slightly distorted but shows a fairly large, Gaussian central lobe at nearly the time determined by the group velocity of the SPP, namely, $t_{\rm SPP} = d/v_{\rm SPP} \approx d/(0.89c) \approx 450(2\pi/\omega_0)$. The reflected SPP and light scattered pulses are highly distorted, and present two lobes (advanced and retarded) stemming from the dip of $R_{\rm SPP}(\omega)$ and $S(\omega)$ at $\omega/\omega_p = 0.275$ [see Fig. 2(b)]. On the other hand, the response of the rectangular ridge, see Fig. 5(b), is much simpler, as expected from the fairly dispersion-less $R_{\rm SPP}(\omega), T_{\rm SPP}(\omega)$, and $S(\omega)$ in Fig. 2, and in agreement with the movie of Fig. 3. All the outgoing pulses preserve the Gaussian shape of the incoming SPP pulse, rescaled by the corresponding coefficients, and with central lobes occurring at the expected times given either by the SPP group velocity (for the reflected and transmitted SPP) or by the speed of light (for the scattered light).

Similar features are in turn observed in the time dependence of the entire angular distribution of the scattered light, $I(\theta,t)$. For the rectangular groove at resonance [see Fig. 6(a)], the entire angular distribution, which consists of a diffraction-like fringe pattern, is distorted along its time evolution; moreover, such distortion differs slightly from one scattering angle to another, thus leading to qualitative changes in the angular distribution. In contrast, the fringe pattern associated with the rectangular ridge [see Fig. 6(b)] evolves uniformly in time according to the Gaussian pulse envelope, as expected.

3.2. Two resonances

An interesting phenomenon, similar to Rabi oscillations, takes place when the incoming SPP simultaneously excites two spectrally close resonances. This is shown in the movie of Fig. 7 for the same rectangular groove but with different pulse parameters: $\omega_0/\omega_p = 0.247$ ($\lambda_0 = 636$

#3513 - $15.00 US Received 12 December 2003; revised 27 February 2004; accepted 27 February 2004
(C) 2004 OSA

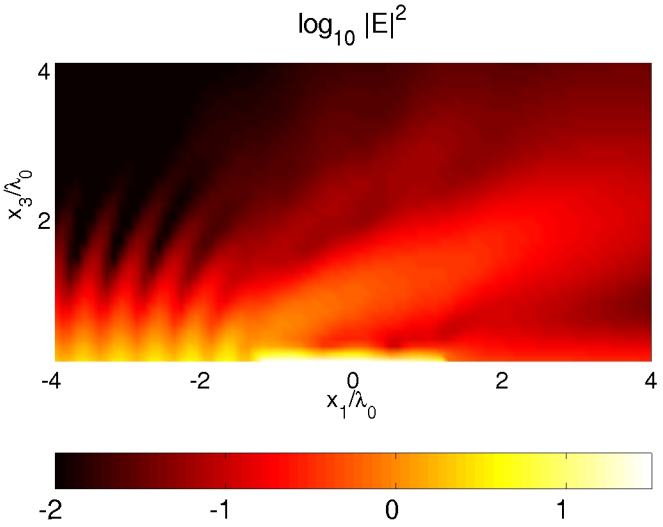

Fig. 7. (328 KB) Same as in Fig. 3 but for different incident SPP pulse parameters: $\omega_0/\omega_p = 0.247$ ($\lambda_0 = 636$ nm) and $\Delta\omega/\omega_0 = 0.035$.

nm) and $\Delta\omega/\omega_0 = 0.035$ (FWHM$\sim$ 39 fs), which ensure that the pulse spectral envelope covers the two resonances at, respectively, $\omega_1/\omega_p = 0.253$ and $\omega_2/\omega_p = 0.241$ (see Fig. 2). The near field maps showing the approach of the incoming SPP and subsequent scattering, before the reflected and transmitted SPP and the scattered light move away from the rectangular defect, are similar to what is shown above for a single resonance. Nevertheless, at longer time steps, the electric field intensity on the defect bounces back and forth from one end of the defect to the other, simultaneously leaking out predominantly from the end with a higher concentration of EM energy density. This is a manifestation of the interference between the two resonances being excited [23].

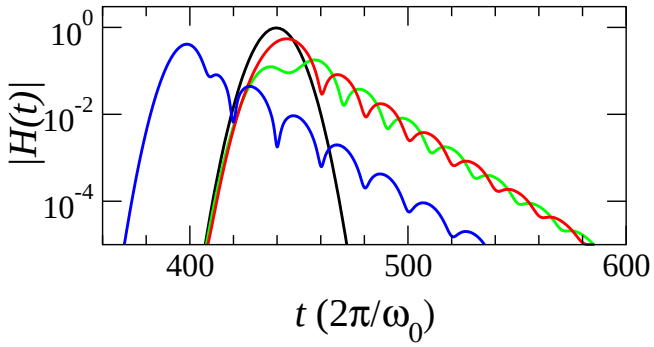

Fig. 8. Same as in Fig. 5(a) but for different incident SPP pulse parameters: $\omega_0/\omega_p = 0.247$ and $\Delta\omega/\omega_0 = 0.035$. $\theta_{max} = 69.6^\circ$.

To quantify the process properly, the time dependence of the magnetic field amplitude of the outgoing pulses is shown in Fig. 8. The Rabi-like oscillations for the reflected and transmitted SPP pulses, and for the scattered light at θ_{max}, are neatly observed superimposed on negative

#3513 - $15.00 US Received 12 December 2003; revised 27 February 2004; accepted 27 February 2004
(C) 2004 OSA

exponential tails at longer times. Such tails provide information on the resonance linewidths and shifts; assuming that both resonances have similar lifetimes, the exponentially decaying envelope yields $\Gamma_1/\omega_0 \approx \Gamma_2/\omega_0 \approx 0.012 \pm 10^{-3}$, whereas the frequency of the oscillations leads to $\omega_1 - \omega_2 \approx 0.05\omega_0 \approx 0.012\omega_p$, in good agreement with the values inferred from Fig. 2.

4. Gaussian groove

For the sake of completeness, and in order to make a comparison with results for grooves of different shape, we present in the movie of Fig. 9 the time dependence of the near field intensity for the resonant scattering of a SPP pulse by a Gaussian groove with parameters corresponding to the resonance studied in Ref. [18] through far field scattering. Qualitatively, the near field intensity behaves as for the single resonance, rectangular groove shown above. Nonetheless, there are some quantitative differences that should be emphasized, which are easily understood in light of the corresponding spectral response of the grooves (see Fig. 2 above and Fig. 1 in Ref. [18]). First, for the Gaussian groove nearly total SPP transmission is observed (negligible SPP reflection and scattered light), whereas a significantly larger percentage of the incoming SPP energy is reflected and scattered (as light), at the expense of lower SPP transmission (though still very large) for the rectangular groove. Second, the Gaussian groove resonance exhibits smaller EM energy concentrations during a substantially shorter lifetime. This is an obvious consequence of the lower-Q value of the excited mode of the Gaussian groove as compared to that of the rectangular groove (at close frequencies), despite being deeper and narrower, revealing the critical role played by the shape of the groove.

5. Conclusions

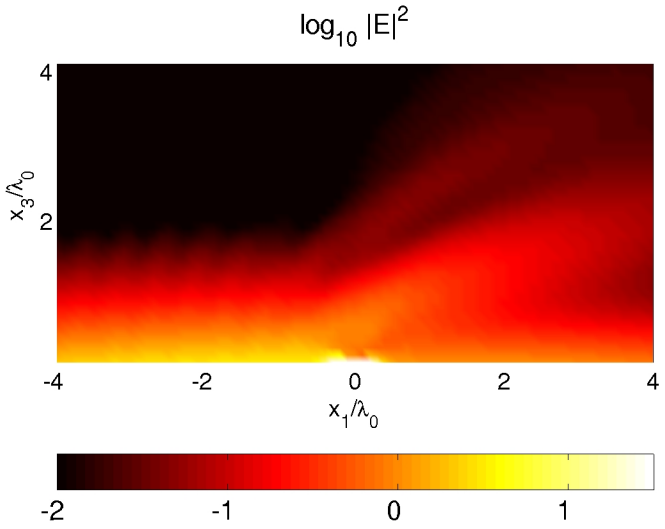

Fig. 9. (252 KB) Movie of the time evolution of the near (electric) field intensity (log scale) images in an area of $8\lambda \times 4\lambda$ perpendicular to the Ag surface for a Gaussian groove (located at the bottom center, see Fig. 1) of $1/e$-width $a = 157$ nm and height $\delta = -785$ nm. The incident SPP pulse parameters are: $\omega_0/\omega_p = 0.239$ ($\lambda_0 = 657$ nm) and $\Delta\omega/\omega_0 = 0.035$. Front picture: $t = 0$ (incoming SPP pulse maximum at $x_1 = 0$).

We have presented a k-space formulation, based on the reduced Rayleigh equation, obtained

#3513 - $15.00 US Received 12 December 2003; revised 27 February 2004; accepted 27 February 2004
(C) 2004 OSA

by means of an impedance boundary condition, for every spectral component of the incoming pulse, which enables us to study the dynamics of the scattering of a pulsed-SPP by a surface profile line defect, both in the far field and in the near field. This formulation has been exploited to investigate the time dependence of the near-field, resonant scattering effects produced at a rectangular groove. The scattering process is tracked through the (time-resolved) repartition of the incoming SPP EM energy into reflected and transmitted SPP pulses, and into pulsed, scattered light. Furthermore, we directly show evidence of the excitation of single resonances, as manifested by the concentration of electric field intensity within the groove during the resonance lifetime and long after the incoming SPP pulse is gone (provided that the pulse width is sufficiently shorter than this lifetime); and then by the subsequent leakage of electric field intensity from the groove, on a time scale also controlled by the resonance lifetime, leading in the far field to exponential tails of the reflected and transmitted SPP pulses, and also of the time dependence of the angular distribution of scattered light. Simultaneous excitation of two resonances is also considered, exhibiting the near-field formation of Rabi-like oscillations. Interestingly, our formulation can be straightforwardly employed to study the near-field (and far-field) dynamics for a finite number of line defects, arbitrarily distributed, which is of much interest in SPP NanoOptics [24]. Extensions to oblique incidence and 2D defects are underway.

Acknowledgments

This work was supported by the Spanish Dirección General de Investigación (Grants BFM2001-2265 and BFM2003-0427) and by the US NSF Grant INT-0084423 and Army Research Office Grant DAAD 19-02-1-0256.

#3513 - $15.00 US Received 12 December 2003; revised 27 February 2004; accepted 27 February 2004
(C) 2004 OSA